Growth behavior of metal-doped silicon clusters SinM (M=Ti,Zr,Hf; n=8-16)

doi: 10.1103/PhysRevB.71.075423

Growth behavior of metal-doped silicon clusters Si_nM (M=Ti,Zr,Hf; n=8–16)

Hiroaki Kawamura,[1] Vijay Kumar,[1,2] and Yoshiyuki Kawazoe[1]
[1]*Institute for Materials Research (IMR), Tohoku University, 2-1-1 Katahira Aoba-ku, Sendai 980-8577, Japan*
[2]*Dr. Vijay Kumar Foundation, 45 Bazaar Street, K.K. Nagar (West), Chennai 600 078, India*
(Received 23 March 2004; revised manuscript received 27 July 2004; published 25 February 2005)

The growth behavior of metal-doped silicon clusters MSi_n, M=Ti, Zr, and Hf and n=8–16 is studied using an *ab initio* ultrasoft pseudopotential plane wave method and the generalized gradient approximation for the exchange-correlation energy. For n=8–12, we find basketlike open structures to be most favorable, while for n=13–16, the metal atom is completely surrounded by silicon atoms. These results are in excellent agreement with the observed reactivity of these clusters. Our results suggest continuous aggregation until n=16, which is the optimal cage for the metal-encapsulated silicon clusters with these elements. Further calculations have been done on cation and anion clusters using the Gaussian method. The calculated electron affinities agree well with experimental results in the range of n=12–16 while the calculated values for smaller clusters are higher. Raman activity and infrared spectra have been calculated for selected clusters. These could help in the identification of the structures of these clusters from experiments.

DOI: 10.1103/PhysRevB.71.075423 PACS number(s): 71.15.Nc, 73.22.−f, 61.46.+w

I. INTRODUCTION

Recent findings[1–7] of metal- (M) doped silicon and germanium clusters have created much interest for the understanding of their properties and growth behavior.[8–16] Experiments on M=Ti, Hf, Cr, Mo, and W doped silicon clusters Si_nM have shown large abundances of n=15 and 16 clusters and low intensities of other clusters.[12,17] In particular, the abundances drop drastically beyond n=16, giving support to the predictions of the exceptional stability of n=16 clusters. These results lend support to the idea[1] that M doping could lead to the production of size-selected silicon clusters in large quantities. The reactivity of Si_nTi clusters decreases sharply beyond n=12, suggesting that the M atom could be surrounded by silicon atoms so that it is not available for reaction.[12] This is in agreement with the calculations that predicted the M atom to be encapsulated within a silicon cage.[1,2] On the other hand, smaller clusters show significant reactivity, suggesting that the M atom could be exposed and available for reaction. An understanding of the growth behavior of these clusters could explain the reactivity results and could lead to general principles of the role of the size and electronic structure in the development of such clusters. Here we present results of a systematic study of the growth behaviors of M=Ti, Hf, and Zr doped silicon clusters. These are in very good agreement with the experimental results of reactivity. Our results show that the large size of the M atom leads to open basketlike structures for $n<13$ so that the M atom is available for reactivity. On the other hand, for larger clusters cage structures are favored in which the M atom is encapsulated in the cage leading to the low reactivity of these clusters.

The electronic structures of Ti-doped silicon clusters have been studied[12] recently with photoelectron spectroscopy and the electron affinities (EAs) have been found to have a minimum at n=16, suggesting the closed electronic shell nature and strong stability of Si_{16}Ti cluster. The electronic, vibrational, and optical properties of $M@Si_{16}$, M=Ti and Zr clusters have also been studied in detail,[14] and the vibrational spectra have been proposed to be a good way to identify the structures of these clusters. The $Ti@Si_{16}$ cluster has been predicted to be luminescent in the blue region, making these clusters attractive for optoelectronic applications. The EA and ionization potential (IP) have been calculated[14] for the $Ti@Si_{16}$ cluster, and the values are 2.05 eV and 7.51 eV, respectively. The calculated EA of $Ti@Si_{16}$ is in good agreement with the experimental value of 1.8 ± 0.1 eV and provides support for the Frank-Kasper (FK) structure of this cluster as the EA of the fullerene (f) isomer is significantly higher (2.85 eV). Therefore EAs of the M-doped clusters could be good guidance for the study of the stabilities and structures of these clusters. We have adopted these strategies to understand the growth behavior of these clusters and have also studied the cation and anion clusters to obtain the EAs and IPs. These are compared with the available experimental data. Further studies of the vibrational spectra have been carried out to check the dynamical stability. The Raman activities and the infrared (IR) intensities have been calculated, which could serve as a guide for experimental verification of the structures of these clusters.

II. METHOD

The calculations on neutral clusters have been performed using the *ab initio* ultrasoft pseudopotential method[18,19] within the spin-polarized generalized gradient approximation of Perdew and Wang[20] for the exchange-correlation energy. In the subsequent discussion, we shall refer to it as PW91PW91. A simple-cubic supercell with size 15 Å for n=8–13 and 18 Å for larger clusters is used with periodic boundary conditions and the Γ point, for the Brillouin zone integrations. For Ti and Zr we treat 3p and 4p atomic core states, respectively, also as valence states. Selected atomic structures of clusters are optimized using the conjugate gradient method to find the lowest-energy structures.

The charged clusters of $Ti@Si_n$ have been studied using

the all electron B3PW91/6-311+G* calculations[21] in the GAUSSIAN 98 code because the experimental results are available on this system. In these calculations, the wave function is represented by a linear combination of atomic orbitals (LCAO). We use the 6-311+G* basis set and hybrid exchange-correlation functional B3PW91 (Becke's three-parameter hybrid functional for exchange[22] and generalized gradient functional of Perdew and Wang for correlation). This LCAO calculation is performed only for the most stable isomers for different sizes that are determined by the plane-wave method calculation. Only in cases where more than one isomer are nearly degenerate are optimizations performed for all such isomers. For obtaining the EA and IP values, the geometries of neutral clusters obtained from the plane-wave method have been reoptimized with the GAUSSIAN 98 code with the above basis set and exchange-correlation functional. In general, deviations from the geometries obtained from the plane-wave method are quite small. The lowest-energy structures as well as most of the other isomers of neutral clusters studied here have zero magnetic moment. The strong interaction between the M and the Si atoms quenches the magnetic moments of the M atom completely. Structures of the ionic clusters have been obtained from the optimizations of the neutral structures. The ground states of the singly charged clusters are doublets. Calculations of the vibrational spectra with Raman activity and IR intensities have been done on neutral clusters using the GAUSSIAN code with the same level of accuracy as that for the optimization of the geometries to test their dynamical stability. This method has been shown[14] to produce excellent results on elemental silicon clusters, in agreement with experiments without using any scaling factor.

III. RESULTS

A. Structures of Si_nM (M=Ti, Zr, and Hf; n=8–16)

One of the smallest clusters for which encapsulation of an M atom could occur is a cube. So we started our search for M-encapsulated clusters from $n=8$ onwards. However, we find that for small sizes any isomer having a cage structure is not favorable and basket structures have the lowest energies. Our calculations show that clusters with $n=8$–12 have basket structures to be the most stable, whereas cage structures are most favorable for $M@Si_n$, $n>12$. The optimized low-lying isomers for M=Ti are shown in Fig. 1 and very similar structures have been obtained for M=Zr and Hf. The binding energies per atom (BEs) and the highest-occupied–lowest-unoccupied molecular orbital (HOMO-LUMO) gaps are given in Table I for M=Ti and in Table II for M=Zr and Hf. Note that in the basket structures the M atom is covered partially with Si atoms and is exposed free (Fig. 1). This is important because in experiments on cation clusters, partially covered M atoms could still have reactivity, while it is unlikely for the cage structures.[23]

The lowest-energy isomers of Si_nM ($n=8$–10, M=Ti, Zr, and Hf) clusters have two Si atoms whose coordination is 2. Such Si atoms are likely to be very reactive and favor further growth of clusters. Although the most stable isomers for $n=11$ and 12 also have basket structures, they are different from $n=8$–10 isomers as all of the Si atoms have higher coordination than 2. This leads to a large increase in the BE from $n=10$ to 11 (0.073 eV/atom), which is the largest among all n and $n+1$ ($n=8$–15) clusters. For sizes $n=13$ and larger, basket structure is not suitable. In the basket structures the number of Si atoms that can interact with the M atom is limited. This fact is reflected by the number of Si atoms that are far from the M atom (over 3.0 Å). These are 1, 2, 2, 4, and 4 for Si_8Ti, Si_9Ti, $Si_{10}Ti$, $Si_{11}Ti$, and $Si_{12}Ti$, respectively. Especially in $Si_{12}Ti$ the capping Si atom on $Si_{11}Ti$ interacts almost only with Si atoms. The result that the basket isomer for $n=12$ has lower energy than cage isomers is interesting and important. In this size range the strong interaction between the Si and the M atoms makes encapsulated silicon clusters more stable as is the case[2,8] for $M@Si_{12}$, M=Cr, Mo, and W. This shows the importance of the size of the M atom in the formation of the caged structures. The Ti atom has a slightly bigger size than Cr, Mo, or W, and therefore in the hexagonal prism structure with Ti at the center, the Si-Si bonds are strained. Its optimized structure is shown in Fig. 1 [n=12(iii)]. The Si-Si bond lengths in the hexagonal prism structure are in the range of 2.32 to 2.46 Å. The length of the elongated (unbonded) Si-Si bond is 3.00 Å. Except for this bond the average Si-Si bond length is 2.37 Å, which is close to the covalent bond length in bulk silicon (2.34 Å). Thus by cutting one Si-Si bond, this isomer does not need to elongate other Si-Si bonds and can keep covalentlike Si-Si bonding in this structure. This indicates that this form is energetically better than keeping all Si-Si bonds strained. We also considered a hexagonal antiprism structure. As shown in Fig. 1 [n=12(v)], in this case the Si-Si bonds can be kept within the two hexagons. However, Si-Si bonds between the hexagons are elongated. The average bond length is 2.49 Å. This and other open structures [12(iv) and 12(vi)] lie significantly higher in energy and are unlikely to be observed in experiments. However, another open structure [12(ii)] lies close in energy with the lowest-energy isomer and may be present in experiments at around room temperature. Similar results have been obtained for Zr and Hf dopings. An open structure was also obtained for $Si_{12}Zr$ by Lu and Nagase[9] with the HOMO-LUMO gap of 0.78 eV using the GAUSSIAN program with a B3LYP hybrid functional and LanL2DZ basis set. However, our lowest-energy isomer has a 1.218 eV HOMO-LUMO gap and is therefore different.

$M@Si_{13}$ has a capped hexagonal prism structure [Fig. 1 n=13(i)] with a large HOMO-LUMO gap (1.569, 1.612, and 1.700 eV for M=Ti, Zr, and Hf, respectively), and this is the first cage structure in the growth process as the lowest energy isomer. All the Si atoms are at a distance of 2.78, 2.85, and 2.83 Å from the Ti, Zr, and Hf atom, respectively. Therefore, a strong interaction is expected between the M and the Si atoms. The average Si-Si bond lengths for M=Ti, Zr, and Hf is 2.47, 2.52, and 2.51 Å. These are elongated compared with the $M@Si_{12}$ hexagonal prism isomer due to the higher coordination of the silicon atoms. A capped hexagonal antiprism [13(ii)] lies 0.380 eV higher in energy. We also studied side capping of a hexagonal prism [13(iii)] as well as an antiprism [13(iv)] and two other structures as shown in Fig. 1. All these lie significantly higher in energy. Interestingly a

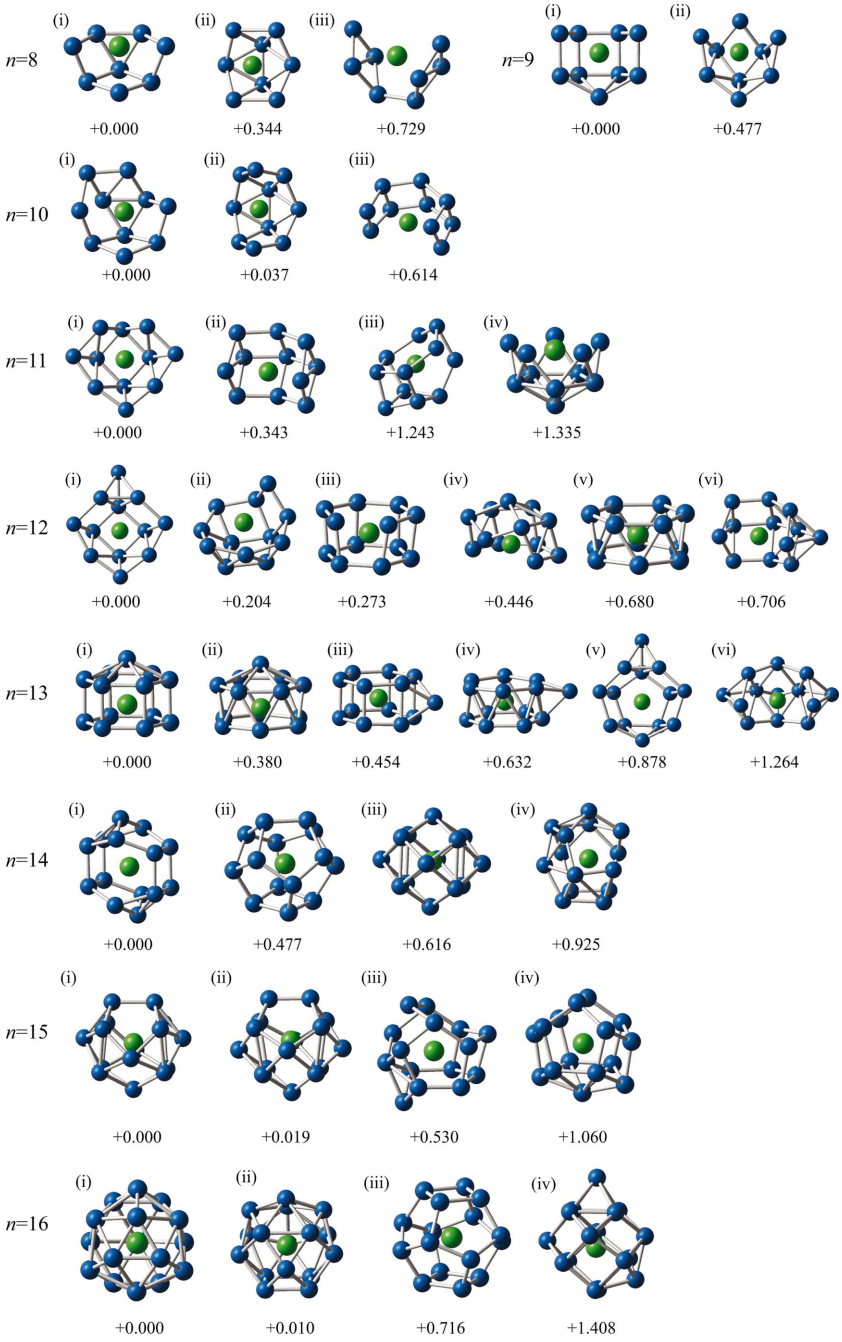

FIG. 1. (Color) Structures and differences of the total binding energies from the most favorable isomer in each size for $Ti@Si_n$ (n=8–16) obtained by using the plane-wave PW91PW91 method. Almost the same structures are obtained for $M@Si_n$ (M=Zr and Hf and n=8–16). Isomers 10(i) and 10(ii) as well as 15(i) and 15(ii) are nearly degenerate. In addition, under experimental conditions of finite temperatures, a few other isomers can coexist such as those with an energy difference of about 0.2 eV in this figure.

cage type structure [13(vi)] lies highest in energy among all the isomers we have studied.

$Ti@Si_{14}$ is a bicapped hexagonal prism structure. The capping Si atoms are not at the centers of the hexagons but displaced symmetrically so that they interact only with four Si atoms and cause large distortions. This is important for the understanding of the reactions. However, because Ti is at the center of the cluster and the maximum Ti-Si bond length is 2.87 Å, Ti could keep bonding with all the Si atoms. Further optimizations of the f cage[24] [n=14(ii)] and a cubic [14(iii)] as well as another isomer lead to structures that are significantly higher in energy. Distorted bicapped hexagonal prism isomers were also obtained earlier[9] for $Zr@Si_{14}$. Structures of $M@Si_{15}$ and $M@Si_{16}$ have been discussed before.[1,3,6,7,14] It is worth mentioning here that there are two nearly degenerate isomers for $M@Si_{15}$, but with significantly different HOMO-LUMO gaps. Their structures [Fig. 1, n=15(i) and (ii)] are almost the same except that the positions of the capping pair of Si atoms and a single atom are interchanged. In Table I we have given the values of the BEs and HOMO-LUMO gaps for these isomers. However, in the B3PW91/6-311+G* calculations the n=15(i) isomer could not be obtained because in the optimization process it transformed into the n=15(ii) isomer. Thus in Table I the results for n=15(i) are shown only for PW91PW91 calculations. Two more isomers have been shown in Fig. 1, but these are significantly higher in energy. The isomers 15(iii) and (iv) can be considered as capped decahedral

TABLE I. Binding energies per atom (BE), the HOMO-LUMO gaps and second-order difference in energy, ΔE^n for neutral clusters obtained from PW91PW91 calculations. The HOMO-LUMO gaps and ΔE^n are also given for neutral, cation, and anion clusters obtained by using B3PW91. The dipole moments on neutral clusters, electronic affinities, and ionization potentials are obtained from B3PW91 calculation. ΔE^n is defined as $\Delta E^n = E(n+1) + E(n-1) - 2E(n)$.

	BE	Gap (eV) (PW91PW91)	Gap (eV) (B3PW91)			ΔE^n (eV) (PW91PW91)	ΔE^n(eV) (B3PW91)			Dipole moment	EA	IP
n	(eV)	Neutral	Neutral	Cation	Anion	Neutral	Neutral	Cation	Anion	(Debye)	(eV)	(eV)
8	3.798	1.233	2.364	1.911	1.598	-	-	-	-	2.062	2.578	6.596
9	3.822	0.986	1.823	1.496	1.632	−0.073	−0.011	−0.774	0.126	0.873	2.963	7.056
10(i)	3.848	1.187	2.186	1.451	1.358	−0.617	−0.733	−0.909	−0.344	1.750	3.012	7.171
10(ii)	3.845	0.732	1.847	1.618	1.607	−0.692	−0.696	−0.076	0.055	0.607	3.192	6.773
11	3.921	1.299	2.242	1.338	1.272	0.386	0.253	−0.179	−1.175	1.359	2.671	7.110
12(i)	3.953	1.257	2.425	1.467	1.467	−0.282	−0.140	0.301	−0.485	1.552	2.424	7.033
12(iii)	3.932	0.763	1.780	1.413	1.313	−0.829	−0.342	−0.473	1.783	1.030	3.660	7.318
13	4.001	1.569	2.668	1.268	1.268	0.322	0.417	−0.130	−0.825	0.539	2.523	7.397
14	4.021	1.451	2.309	1.471	1.201	−0.626	−0.649	−0.381	−0.718	0.009	2.729	7.214
15(i)	4.077	1.578	-	-	-	−0.136	-	-	-	-	-	-
15(ii)	4.076	1.237	2.192	1.399	1.258	−0.173	0.075	−0.148	0.422	1.043	2.874	7.299
16(i)	4.135	2.358	3.468	1.368	1.171	-	-	-	-	0.004	2.051	7.514
16(iii)	4.093	1.492	2.475	1.366	1.418	-	-	-	-	0.026	2.853	6.981

structures. It is interesting to note that for M-encapsulated clusters of germanium, decahedral isomers become favorable.[5] The lowest-energy isomer for $Ti@Si_{16}$ is a Frank-Kasper polyhedron [16(i)]. Another isomer in which the triangle along the three-fold symmetric axis in 16(i) is rotated by 30° is nearly degenerate. The latter [16(ii)] is the ground state for M=Hf. The fullerenelike isomer [16(iii)] of $Ti@Si_{16}$ lies 0.716 eV higher, but it is

TABLE II. The same as in Table I but for Si_nZr and Si_nHf isomers obtained from PW91PW91 calculations. Their optimized structures are almost the same as for Si_nTi. Labels (i)–(v) correspond to the structures in Fig. 1.

	Zr				Hf	
Size	BE (eV)	ΔE^n (eV)	Gap (eV)	BE/atom (eV)	ΔE^n (eV)	Gap (eV)
8(i)	3.922		1.387	3.893		1.225
9(i)	3.905	−0.610	0.994	3.903	−0.255	0.998
10(i)	3.946	−0.184	1.344	3.934	−0.351	1.215
10(iii)	3.888	−1.462	1.164	3.891	−1.295	1.104
11(i)	3.996	0.364	1.356	3.989	0.337	1.353
12(i)	4.011	0.490	1.218	4.010	0.033	1.239
12(iii)	3.961	−0.810	0.770	3.981	−0.714	0.832
12(v)	3.932	−1.550	0.467	3.950	−1.529	0.300
13(i)	3.988	−1.082	1.612	4.026	−0.489	1.700
13(ii)	3.976	−1.416	0.673	4.004	−1.092	0.744
13(v)	3.971	−1.558	0.636	3.984	−1.654	0.659
14(i)	4.040	−0.006	1.377	4.072	0.409	1.395
15(i)	4.083	−0.703	1.551	4.083	−1.396	1.572
15(ii)	4.086	−0.590	1.287	4.086	−1.284	1.262
15(iii)	4.083	−0.710	1.179	4.083	−1.404	1.175
16(i)	4.141		2.448	4.171		2.352
16(iii)	4.162		1.580	4.175		1.576

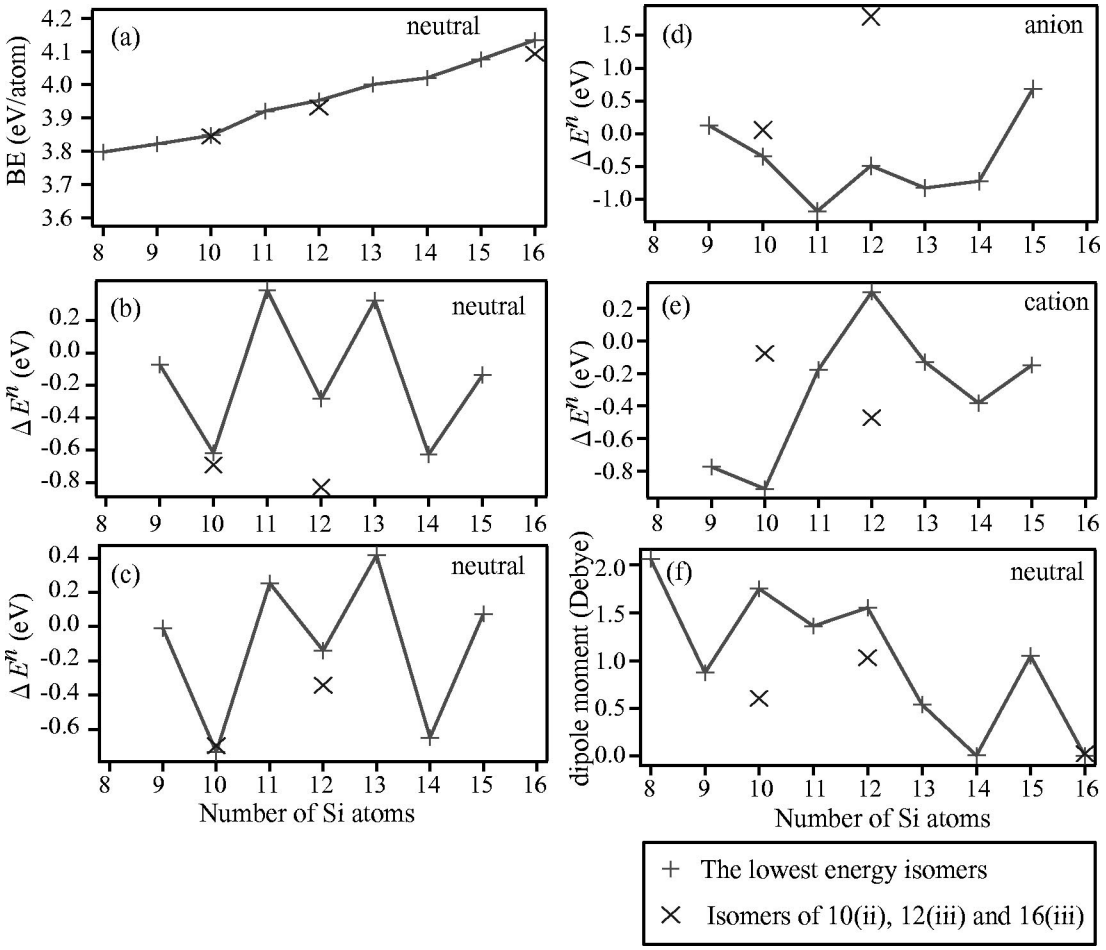

FIG. 2. (a) Binding energies divided by the number of atoms $N(=n+1)$ obtained by using PW91PW91, ΔE^n for neutral clusters obtained by (b) PW91PW91 and (c) B3PW91. (d) and (e) show the results for the charged clusters obtained by B3PW91. (f) shows the dipole moments for neutral clusters obtained by B3PW91. ΔE^n is defined in Table I.

the ground state for Zr-doped cage. For Hf the two isomers are nearly degenerate but their HOMO-LUMO gaps are quite different. Another structure that can be described as capped body-centered-cubic structure [16(iv)] lies 1.408 eV higher in energy than the lowest-energy isomer for $M=$Ti.

B. Energetics and growth behavior

From Tables I and II the energetic and growth behaviors of the clusters can be discussed. The BE increases with size and there is no peak in the range of $n=8$–16 for $M=$Ti so that the clusters can continue to gain energy as their growth proceeds and therefore steady growth would be expected [Fig. 2(a)]. This result agrees with experiments that show high-intensity peaks only for $Ti@Si_{15}$ and $Ti@Si_{16}$ and much weaker intensities for other clusters. It was shown[1] earlier that the energy to add one Si atom to a $M@Si_{16}$ cluster is significantly smaller than the BEs of the $M@Si_n$ clusters, and this leads to the magic behavior of the 16-atom cluster and it also implies that the growth will saturate at $n=16$ as the 16-atom cage is the maximum size possible around a Ti atom. The second-order difference in energy $\Delta E^n=E(n+1)+E(n-1)-2E(n)$ is positive also for $n=11$ and 13 [Fig. 2(b)], indicating their magic nature. A similar result has been obtained [Fig. 2(c)] from the B3PW91/6-311 +G* calculations. However, in experiments $n=11$ and 13 are not very abundant. This is due to the charged nature of the clusters. The experiments[12] on anion clusters show only $n=15$ and 16 to be strongly abundant. As discussed below the anion clusters with $n=11$ and 13 are not magic [see Fig. 2(d)] while $n=15$ is strongly magic. On the other hand, for cation clusters $n=12$ becomes magic while $n=15$ is not. Therefore, the abundance of clusters is expected to be dependent on the charged state. Interestingly for anion clusters our results also indicate only $n=15$ and 16 to be magic, giving these clusters strong size selectivity. The magic nature also changes if other isomers are present in experiments and this could lead to some variations in the intensities as compared to what may be expected on the basis of the lowest energy structures. Also the neutral clusters in general have large permanent dipole moments and this is shown in Fig. 2(f). However, for the symmetric clusters such as $n=14$ and 16, this becomes zero as it has been shown[25] recently for Nb clusters.

The BE in the case of $M=$Hf also increases monotonically (Table II). However, for $M=$Zr, the BE decreases slightly in going from Si_8Zr to Si_9Zr and from $n=12$ to 13.

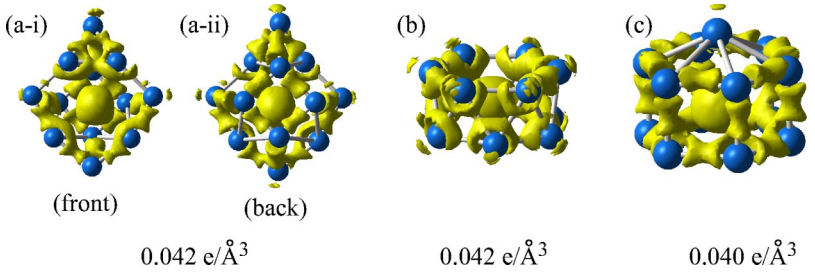

FIG. 3. (Color online) Constant electronic charge density surfaces for the (a) $Si_{12}Ti$ basket isomer, (b) $Ti@Si_{12}$ hexagonal antiprism isomer, and (c) $Ti@Si_{13}$ capped hexagonal prism isomer.

Therefore, M=Zr doping is likely to show slightly different abundances. The second-order difference in energy shows n=11 and 12 to be magic for Zr while 11 and 14 are magic for Hf. Therefore, even though the structures for these different M atoms are similar, the abundance behavior can be expected to be slightly different. In most cases the HOMO-LUMO gaps are around 1.3 eV within PW91PW91. However, the FK isomer of n=16 has the largest gap.

As mentioned before, the basket structures are the best for small clusters. Therefore, the size at which the cage structure is formed has great importance for the understanding of their growth behavior and reactivity. For n=8–10 we also tried cubic and capped structures as well as pentagonal prism and antiprism structures all of which transform into basket structures when optimized and no cage structure is obtained. In these isomers Si atoms are too few to surround the M atom so that every time the structure is optimized, the M atom comes out of the cage of the cluster and appears on the surface. This could easily be confirmed from Fig. 1 n=10(iii) and n=11(iv), which show some of the optimized cagelike structures. Therefore, for n=8–10 cage structures do not exist and there is no local minimum isomers. For n=11 a cagelike structure [Fig. 1 n=11(iii)] has been obtained only for Ti-doped clusters. However, its BE is quite low as compared to the value for the basket isomer and therefore this is unlikely to be present in experiments. For n=12, as discussed above, the basket isomer has the lowest energy and the difference of total energy between the basket and the hexagonal prism isomers is only 0.273 eV. This indicates that cage isomer may exist in experiments. On the other hand, at n=13 the total energy difference between the basket and the cage structures is not small (0.878 eV) and therefore formation of the basket isomer is very unlikely. This is in excellent agreement with experimental results of Ohara *et al.*,[12] who studied the reaction of cation clusters with H_2O to confirm cage structures of the clusters and found that $Ti@Si_n^+$ (n=13–17) clusters have little reactivity with H_2O, while clusters with n=7–12 are quite reactive. Therefore, transformation from a basket to a cage structure should occur in going from n=12 to 13. In the size range of n=13–17, in experiments n=14 has relatively more reactivity. This is because the n=14 cage isomer (Fig. 1) has two open hexagons and a distorted structure that is more reactive.[23] Furthermore, n=13 cluster has one uncapped open hexagon and its reactivity is about half of n=14. Considering closed cage structures for n=15 and 16 and the fact that there was almost no reactivity for these clusters in the experiment, we conclude that it is necessary for the M atoms to remain exposed for reactivity and that the effect of charge on the reactivity of the clusters is negligible. Detailed calculations[23] of the interaction of water on these clusters have also supported the experimental findings.

C. Bonding nature and electronic structure

In order to understand the bonding nature in these clusters, we show in Fig. 3 the constant electronic charge density isosurfaces for the basket, hexagonal prism, and antiprism isomers of $Si_{12}Ti$. The basket isomer has different bonding natures in different regions and therefore two different views are shown. The front view shows eight Si atoms in Fig. 3(a-i) that have covalent metallic character. The electronic charge density shows covalent bonding between the Si atoms that are partially attracted towards the M atom. In the back view there are four bottom Si atoms with covalent bonding [Fig. 3(a-ii)] and no charge is seen between the silicon and the M atoms. Thus four Si atoms have a slightly weak interaction with Ti compared to the other eight Si atoms.

The hexagonal antiprism isomer has a completely different bonding character. As one can easily see in Fig. 3(b) the charge density is distributed around Si atoms and no charge is found between the Si atoms at this density (0.042 Å^3). Thus the bonding has metallic behavior and this is due to the high coordination of Si atoms. On the other hand, in the hexagonal prism isomer [Fig. 3(c)] of $Ti@Si_{13}$, Si-Si bonds have strong covalent character except for those connected with the capping atom. Because the doped M atom is located near the bottom of the prism, the electronic charge density of Si atoms consisting of the bottom hexagon is slightly attracted to the M atom. A high-electron-density region could not be found around the capping Si atom. This would mean that the capping Si atom bonds equally to 6 Si atoms and its bonding character is metallic. A similar behavior was earlier noted[1] for the FK isomer of $Ti@Si_{16}$, which also has four capped hexagons. On the other hand, the fullerenelike isomer has covalent bonding as discussed before.[1]

The orbital energies of the neutral clusters are shown in Figs. 4 and 5 by using a Gaussian broadening. Clusters with n=8 and 10–16 have large HOMO-LUMO gaps and for n=16 the HOMO-LUMO gap is exceptionally large. As shown elsewhere,[14] it makes this cluster luminescent in the blue region. Other clusters and particularly the one with n=13 is also likely to be luminescent in the visible range. The results of the B3PW91/6-311+G* calculations show much larger HOMO-LUMO gaps than the values one normally would expect. As an example in the PW91PW91 calculation the HOMO-LUMO gaps for 10(ii) and 12(iii) are 0.732 and 0.763 eV, but in B3PW91/6-311+G* calculations, the val-

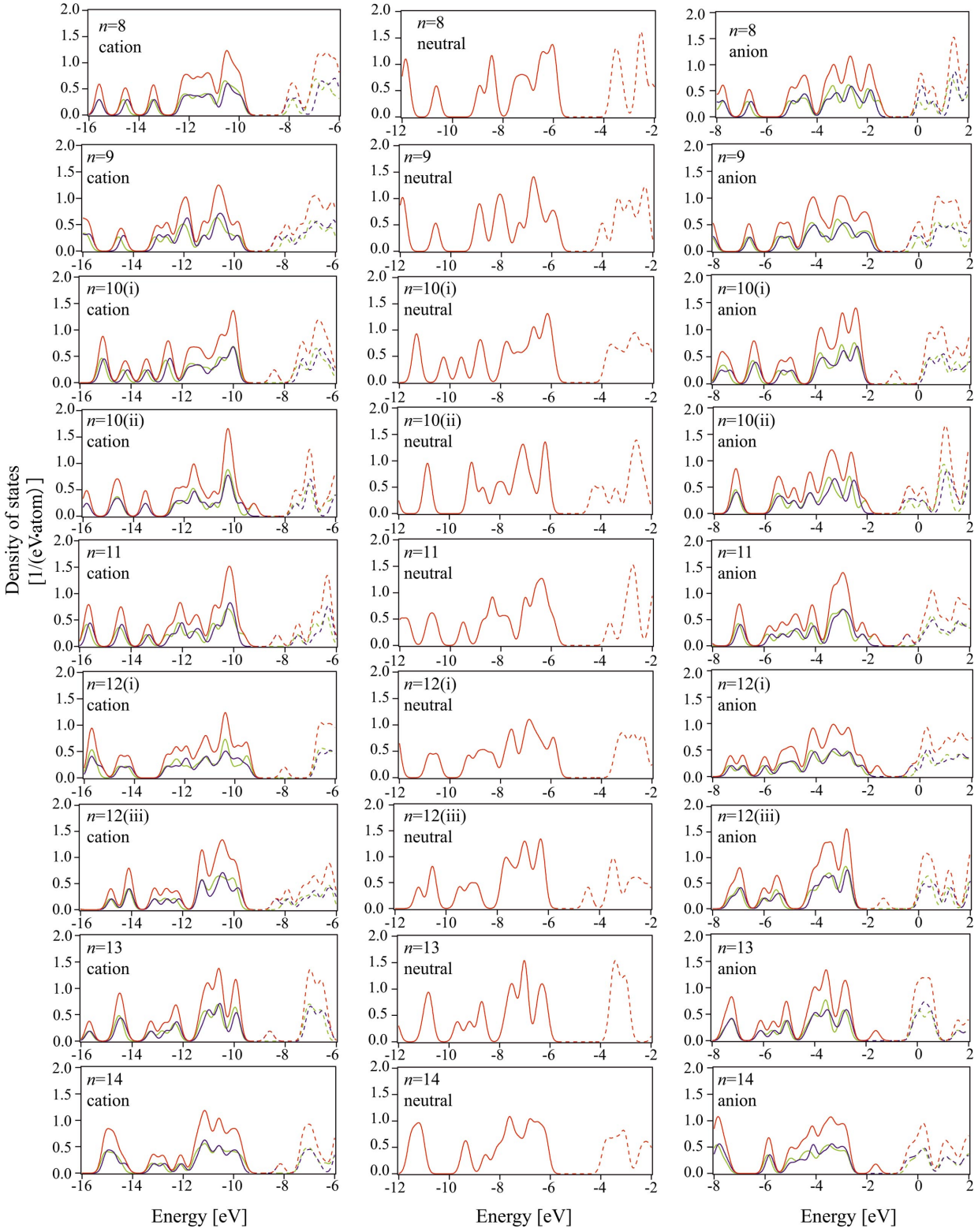

FIG. 4. (Color) Gaussian broadened electronic spectra of Si_nTi ($n=8$–14) clusters. The unoccupied states are shown by broken curves. Red, green and blue lines show total, up-spin and down-spin states, respectively. The nomenclature of the isomers is according to Fig. 1.

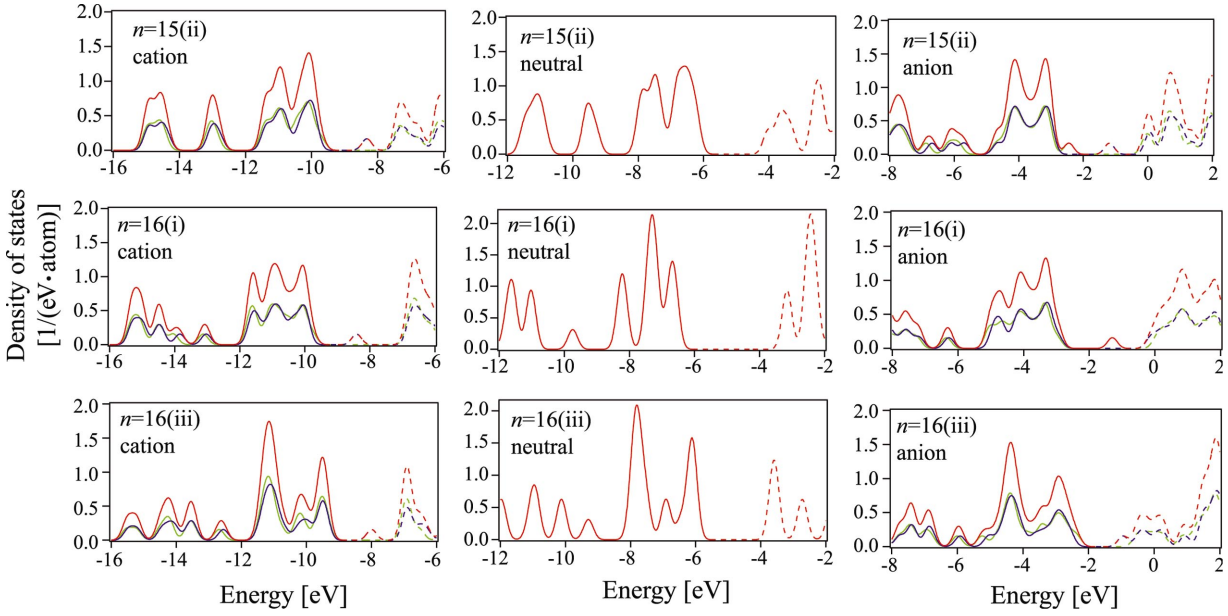

FIG. 5. (Color) The same as in Fig. 4 but for $n=15$ and 16.

ues are 1.847 and 1.780 eV, respectively. Test calculations on the fullerene isomer of $Ti@Si_{16}$ using the plane-wave pseudopotential method with the PW91PW91 functional give the HOMO-LUMO gap to be 1.496 eV while the HOMO-LUMO gap from the all-electron PW91PW91/6-311+G* calculation is 1.474 eV. These results suggest that the effect of the basis set on the HOMO-LUMO gap is small and the choice of the exchange-correlation functional is important for the proper understanding of these clusters, though the structural features seems to be less sensitive to it.

D. Charged clusters

The study of the effects of charging the clusters is important in order to compare with experimental results because experiments are done on cation or anion clusters. The EA and photoemission measurements[12] have been done on these clusters. We have calculated properties of cation and anion clusters to obtain both the EAs and IPs as well as their relative stabilities. Figures 4 and 5 show the Gaussian broadened orbital energies of the charged $Ti@Si_n$ ($n=8$–16) clusters. In the case of cation clusters the spectra shift to higher binding energies and one orbital energy lies in the HOMO-LUMO gap in most cases. This leads to a significant reduction in the HOMO-LUMO gap (Table I) in general. However, in some cases the change is small such as for $n=9$, 10(ii), and 12(iii). In the case of the anion clusters, a small peak appears just above the HOMO level of the neutral clusters in most cases and the spectra shift to lower binding energies. In general, the peaks become broader due to the splitting of the spin-up and spin-down orbital energies. However, in some cases such as the 10(ii) cation, one of the peaks becomes sharper. Experimental results of photoemission do not show much structure and therefore a detailed comparison is not possible.

$Si_{10}Ti$ has two nearly degenerate structures [Fig. 1 $n=10$(i) and 10(ii)] but the relative stabilities of the charged clusters change (Fig. 2). As seen in Fig. 4, the anion and cation of $n=10$(ii) have large gaps due to the large exchange splittings. The gaps have the second largest values among all cation and anion clusters we have studied. On the other hand in the case of $n=10$(i), anion and cation clusters have LUMO states that lie almost in the middle of the HOMO and LUMO of the neutral cluster so that HOMO-LUMO gaps for the anion and cation of this isomer are small. Thus the isomer $n=10$(ii) is more stable when it is charged as it is also seen from the second-order difference in energy [Figs. 2(d) and 2(e)]. A comparison with the stability of the hexagonal prism $Ti@Si_{12}$ structure [Fig. 1 $n=12$(iii)] shows an interesting behavior. The neutral and anion clusters of this isomer do not have large gaps, and compared with the basket isomer, the cage structure is less stable for the neutral. However, the anion of the cage isomer has significantly higher stability [Fig. 2(d)] than that of the basket isomer. This is because the anion has a more regular hexagonal prism structure, while the neutral and cation clusters have elongated Si-Si bonds in the prism structure. The stability of the $Ti@Si_{16}$ cation should also be mentioned. $Ti@Si_{16}$ has two structures: (1) the FK isomer 16(i) and (2) the fullerene isomer 16(iii). The FK isomer is more stable when the clusters are neutral. However, the lowest-energy structures of the cation and anion are both fullerenelike. The differences in the total energy between the fullerene and FK isomers are 0.353 eV for the cation and 0.621 eV for the anion clusters.

The EAs and IPs of the Si_nTi clusters are given in Table I. The EA of $Ti@Si_{16}$ is the lowest and it agrees well with the experimental value of 1.81 ± 0.1 eV. Also the calculated values of 2.671, 2.424, 2.523, 2.729 and 2.874 eV for the EAs of $n=11$–15 clusters agree well with the experimental value of 2.45 ± 0.15, 2.56 ± 0.17, 2.59 ± 0.15, 2.56 ± 0.15, and 2.78 ± 0.13 eV. However, for $n=8$–10, the calculated values are about 0.6 eV higher than the highest experimental results. It is likely that a more accurate treatment of the correlations may be important for some of these small clusters. The EA of

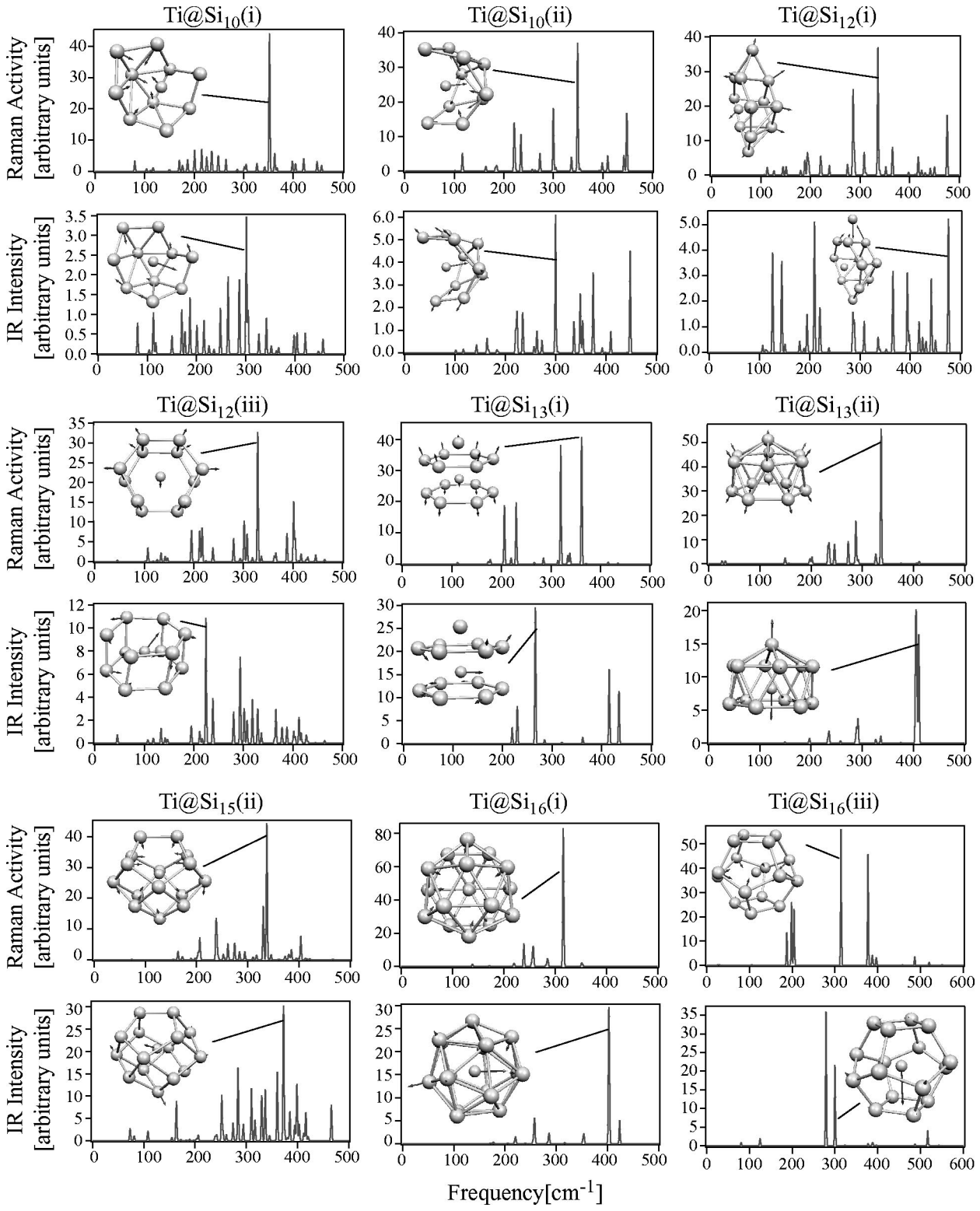

FIG. 6. Gaussian-broadened Raman activity and infrared intensity for $Ti@Si_n$ ($n=10$, 12, 13, 15, and 16). Insets show the displacements of the ions in the frequency modes having the highest activity or intensity.

the hexagonal prism isomer of $n=12$ is the largest, which also explains why its anion becomes very stable. The IPs of these clusters are generally high and the highest value of 7.514 eV is obtained for $n=16$, reflecting its strong magic behavior.

E. Vibrational spectra

In order to further check the dynamical stability of the clusters, we calculated the vibrational spectra. The Raman and IR spectra for $n=10$, 12, 13, 15 and 16 clusters are

TABLE III. Dominant Raman and infrared (IR) frequencies (ω), IR intensities (I), and Raman activity (A) for Si_nTi [$n=10$(i), 10(ii), and 12(i)].

$Si_{10}Ti$ (i)			$Si_{10}Ti$ (ii)			$Si_{12}Ti$ (i)		
ω (cm^{-1})	Raman A (Å^4/amu)	IR I (km/mol)	ω (cm^{-1})	Raman A (Å^4/amu)	IR I (km/mol)	ω (cm^{-1})	Raman A (Å^4/amu)	IR I (km/mol)
80.2	8	2	116.4	13	0.4	126.3	3	9.8
112.4	1	3	220.6	19	2.5	144.5	6	8.9
170.1	9	3	221.5	19	0.0	193.7	14	0.0
186.8	9	4	223.2	4	4.5	209.6	0	12.8
200.9	17	2	234.6	26	4.4	220.2	10	3.9
215.2	18	2	272.9	13	1.4	286.0	62	3.8
235.6	16	0	299.9	46	15.3	288.7	16	3.1
248.7	12	3	336.5	10	3.5	308.4	17	3.1
264.3	9	5	349.0	93	6.6	336.1	93	1.5
287.2	2	5	374.7	0	8.9	365.6	21	8.0
301.4	4	9	409.7	11	2.4	394.3	0	7.8
304.9	6	3	442.4	11	0.1	441.8	5	7.3
352.1	111	1	448.2	42	11.3	475.9	43	13.1

shown in Fig. 6. We have also shown the direction of motion of the ions for the frequency with the highest Raman activity or IR intensity for each cluster. The dominant peaks are also given in Tables III, IV, and V. As seen in the insets in Fig. 6, the vibrations of the M ion contribute dominantly to the IR spectra, while the vibrations of the Si cage ions contribute to the Raman activity. Raman activity mainly corresponds to the breathing modes and in these modes all the ions in clusters having high symmetry move together, as it is the case[14] for $Ti@Si_{16}$, which has a sharp peak in the Raman activity at 316.1 cm^{-1} due to the high symmetry of this cluster. This peak splits into two in the case of the fullerenelike isomer due to the reduced symmetry and the change in the bonding nature so that the atoms within the two squares bind more strongly with the remaining ring atoms. It leads to a higher-frequency mode, while the lower-frequency modes correspond to the motions of the ions on the ring. A similar mode is also seen in $n=13$(i), 13(ii), and 15(ii) isomers. Though $Ti@Si_{12}$(iii) has a hexagonal prism structure, the bonding between Si atoms is not homogeneous and there are many frequency modes in the Raman spectrum due to distortions. On the other hand, $Ti@Si_{13}$ has a capped hexagonal prism structure and there are only a few modes reflecting the high symmetry of this cluster. In the case of $Ti@Si_{13}$(i) the high-

TABLE IV. Same as in Table III but for $Ti@Si_n$ [$n=12$(iii), 13(i), and 13(ii)].

$Ti@Si_{12}$(iii)			$Ti@Si_{13}$(i)			$Ti@Si_{13}$(ii)		
ω (cm^{-1})	Raman A (Å^4/amu)	IR I (km/mol)	ω (cm^{-1})	Raman A (Å^4/amu)	IR I (km/mol)	ω (cm^{-1})	Raman A (Å^4/amu)	IR I (km/mol)
195.6	13	0	205.9	24	0	201.8	7	0
212	20	3	206.2	24	0	232.9	17	2
216.7	22	1	229.6	25	10	235.2	19	4
224.5	0	27	230.1	25	11	245.4	11	0
238.6	9	10	265.9	1	39	245.9	11	0
280.3	15	7	266.6	0	39	272.4	23	0
293.5	2	19	319.7	96	1	287.2	44	1
301.7	26	7	333.9	4	0	289.1	3	6
307.4	18	5	334.3	4	0	291.8	4	9
318.2	2	9	338.2	4	0	325.7	6	0
329	82	8	338.5	4	0	326.6	6	1
365.7	5	7	361.9	102	3	336.4	139	3
388.1	18	4	415.1	1	22	404.8	0	39
401.5	38	3	415.7	1	20	406.5	0	34
404.5	14	1	435.1	1	28	410.7	2	41

TABLE V. Same as in Table III but for $Ti@Si_n$ [$n=15$(ii), 16(i), and 16(iii)].

	$Ti@Si_{15}$(ii)			$Ti@Si_{16}$(i)			$Ti@Si_{16}$(iii)	
ω (cm^{-1})	Raman A (Å^4/amu)	IR I (km/mol)	ω (cm^{-1})	Raman A (Å^4/amu)	IR I (km/mol)	ω (cm^{-1})	Raman A (Å^4/amu)	IR I (km/mol)
163.7	7	22	239.2	18	0	187.3	34	0
206.4	18	3	239.6	18	0	198.2	33	0
237.9	28	0	256.1	11	4	198.6	33	0
239.5	18	2	257.4	15	8	203.9	31	0
252.2	4	25	258.1	15	6	204.6	31	0
283.8	7	41	284.8	5	1	278.7	0	45
310.1	2	29	285.4	6	2	279.2	0	48
330.2	41	21	286.5	5	4	299.8	0	54
337	111	29	316.1	180	0	314.2	141	0
360.4	0	38	316.5	23	0	377.0	43	1
372.6	3	76	317.4	15	0	377.3	73	1
384.9	8	16	402.4	0	26	388.2	7	0
398.8	1	32	402.4	0	29	396.3	4	0
403.2	19	9	403.3	0	25	516.3	0	6
465.9	0	20				516.7	0	5

est Raman activity is at 361.9 cm^{-1}. This is higher than the highest values for $n=10$(i), 10(ii), 12(i), and 12(iii) isomers and it indicates high stability and the magic nature of this cluster.

In the IR spectra the ions move in various directions in many clusters in the most intense mode. However, in $Si_{10}Ti$ (i) and (ii) Si ions move in the direction opposite to that of the Ti ion in the highest-intensity mode so that this is a breathing mode. In experiments these spectra could be a clue to distinguish isomers of the same size cluster. Comparing the frequencies of $n=10$(i) and 10(ii) isomers, both of which have the highest intensity at almost the same frequencies, namely (i) 352.1 and (ii) 349.0 cm^{-1} in the Raman spectra and (i) 301.4 and (ii) 299.9 cm^{-1} in the IR spectra, it will be difficult to identify the isomers on the basis of these modes. However, the intensities for the high-frequency modes for the two isomers differ significantly and could be used for the identification. $Si_{10}Ti$ (ii) has high intensity of the high-frequency IR modes (448.2 cm^{-1}) due to its high symmetry, while $Si_{10}Ti$ (i) does not have such a high-intensity high-frequency mode. Similarly the differences in the $Si_{12}Ti$ (i) and $Si_{12}Ti$ (iii) isomers are clearly seen in the IR spectra. In the Raman spectra the highest-activity modes have nearly the same frequencies, viz., (i) 336.1 and (iii) 329.0 (cm^{-1}). On the other hand, in the IR spectra, the intensities are quite different. $Si_{12}Ti$ (i) has several dominant modes from low to high frequencies and the highest intensity is for the significantly high-frequency mode (475 cm^{-1}). This corresponds to the motion of a few low coordinated atoms. On the other hand, the $Ti@Si_{12}$(iii) isomer does not have any such high-frequency mode. The highest IR intensity mode is at 224.5 cm^{-1} and the highest Raman activity is at 329 cm^{-1}. The intensities of the other high-frequency modes decrease. For $n=13$ and 16, there are only a few high-intensity modes so that they could be easily distinguished from Raman or IR spectra.

IV. SUMMARY

In summary, we have reported detailed *ab initio* calculations of Ti-, Zr-, and Hf-doped silicon clusters and discussed in detail the structures, binding energies, electron affinities, ionization potentials, and Raman and infrared spectra particularly for Ti-doped clusters. $Ti@Si_n$ clusters form basket structures up to $n=12$ and cage structures from $n=13$ onwards. The best cage is obtained for $n=16$, which is a strongly magic cluster and our results are in general agreement with the experiments that find high abundances of 15 and 16 anion clusters with low intensities of others. The size at which cage isomers are formed is also in good agreement with experimental results. The electron affinities are also in good agreement with experiments except for the small clusters with 8–10 Si atoms. The anion of $Ti@Si_{12}$ shows high stability due to the transformation of its structure to a more symmetric hexagonal prism structure. Thus $Ti@Si_{12}$ hexagonal prism isomer has high electron affinity. Infrared intensities and Raman activities show distinct spectra for these clusters, which also reflect the changing bonding nature. These can be used to identify the structures of these clusters from experiments.

Note added in proof. Recently, high intensities of $Ti@Si_{16}$ neutral clusters have been obtained with very low intensities of other Ti-doped silicon clusters[26] confirming the predictions (Ref. 1 and this paper) of high stability and magic behavior of this cluster.

ACKNOWLEDGMENTS

V.K. gratefully acknowledges the kind hospitality at the Institute for Materials Research of the Tohoku University. We are grateful to the staff of the Center for Computational Materials Science at IMR for making the Hitachi SR8000 supercomputer available.

[1] V. Kumar and Y. Kawazoe, Phys. Rev. Lett. **87**, 045503 (2001); **91**, 199901(E) (2003).
[2] H. Hiura, T. Miyazaki, and T. Kanayama, Phys. Rev. Lett. **86**, 1733 (2001).
[3] V. Kumar and Y. Kawazoe, Phys. Rev. B **65**, 073404 (2002).
[4] V. Kumar and Y. Kawazoe, Appl. Phys. Lett. **83**, 2677 (2003); V. Kumar, A. K. Singh, and Y. Kawazoe, Nano Lett. **4**, 677 (2004); V. Kumar, C. Majumder, and Y. Kawazoe, Chem. Phys. Lett. **363**, 319 (2002).
[5] V. Kumar and Y. Kawazoe, Phys. Rev. Lett. **88**, 235504 (2002).
[6] V. Kumar, Eur. Phys. J. D **24**, 81 (2003); Comput. Mater. Sci. **30**, 260 (2004).
[7] V. Kumar, Bull. Mater. Sci. **26**, 109 (2003).
[8] V. Kumar and Y. Kawazoe, Phys. Rev. Lett. **90**, 055502 (2003).
[9] J. Lu and S. Nagase, Phys. Rev. Lett. **90**, 115506 (2003).
[10] F. Hagelberg, C. Xiao, and W. A. Lester, Jr., Phys. Rev. B **67**, 035426 (2003).
[11] S. N. Khanna, B. K. Rao, and P. Jena, Phys. Rev. Lett. **89**, 016803 (2002).
[12] M. Ohara, K. Koyasu, A. Nakajima, and K. Kaya, Chem. Phys. Lett. **371**, 490 (2003).
[13] S. N. Khanna, B. K. Rao, P. Jena, and S. K. Nayak, Chem. Phys. Lett. **373**, 433 (2003).
[14] V. Kumar, T. M. Briere, and Y. Kawazoe, Phys. Rev. B **68**, 155412 (2003).
[15] Z. Chen, A. Hirsch, S. Nagase, W. Thiel, and P. von Rague Schleyer, J. Am. Chem. Soc. **125**, 15507 (2003).
[16] P. Sen and L. Mitas, Phys. Rev. B **68**,155404 (2003).
[17] S. M. Beck, J. Chem. Phys. **90**, 6306 (1989).
[18] G. Kresse and J. Hafner, J. Phys.: Condens. Matter **6**, 8245 (1994).
[19] D. Vanderbilt, Phys. Rev. B **41**, 7892 (1990).
[20] J. Perdew, *Electronic Structure of Solids '91*, edited by P. Ziesche and H. Eschrig (Akademie Verlag, Berlin, 1991).
[21] M. J. Frisch *et al.*, *Gaussian 98, Revision A.11.1* (Gaussian, Inc., Pittsburgh, PA, 2001).
[22] A. D. Becke, J. Chem. Phys. **98**, 5648 (1993).
[23] H. Kawamura, V. Kumar, and Y. Kawazoe, Phys. Rev. B (to be published).
[24] T. Miyazaki, H. Hiura, and T. Kanayama, Phys. Rev. B **66**, 121403 (2002).
[25] K. E. Andersen, V. Kumar, Y. Kawazoe, and W. E. Pickett, Phys. Rev. Lett. **93**, 246105 (2004).
[26] K. Koyasu, Y. Naono, M. Akutsu, and A. Nakajima [results reported in ISSPIC 12 Conference in Nanjing (2004)].